WATER RESOURCES RESEARCH, VOL. 25, NO. 6, PAGES 1195–1207, JUNE 1989

Wetting Front Instability
2. Experimental Determination of Relationships Between System Parameters and Two-Dimensional Unstable Flow Field Behavior in Initially Dry Porous Media

R. J. GLASS,[1] T. S. STEENHUIS, AND J-Y. PARLANGE

Department of Agricultural and Biological Engineering, Cornell University, Ithaca, New York

This paper describes and interprets experimental studies of wetting front instability guided by the dimensional analysis presented in paper 1 (R. J. Glass et al., this issue). When a wetting front passes from a fine-textured layer of initially dry sand into an underlying coarse layer, the front breaks into fingers. A specially developed vertical slablike chamber and associated techniques were developed for the study of such fingering. The flow rate through the system is systematically varied by using different mean grain size separates for the upper layer (the same coarse separate being used for the bottom layer). Relationships between finger width, propagation velocity, moisture content, and flow rate through individual fingers are experimentally determined and related to the properties of the bottom layer and the flow rate through the system. The results are different than those found in a previous experimental study which used different techniques for sample preparation. Results obtained here agree with a formulation derived earlier by J-Y. Parlange and D. E. Hill (1976) through linear stability analysis.

INTRODUCTION

In paper 1 [*Glass et al.*, this issue] (hereafter referred to as P1) it is argued that the stability of a given vertical infiltration system is a function of the expected finger width in two-dimensional systems (or diameter in three dimensions) calculated for the layer and the maximum horizontal width (or diameter) of the system. If the finger width is less than the width of the system then instability is expected, while for a finger width greater than or equal to the maximum system width the system is stable. Through dimensional analysis at the finger scale, finger width, d, in an isotropic and homogeneous porous media was shown to be

$$d = \frac{S^2}{(\theta_s - \theta_i)K_s} f_{dF}(R_F) \tag{1}$$

where θ_s and θ_i are the saturated and initial moisture contents, respectively, K_s is the saturated conductivity, S is the sorptivity evaluated between θ_i and θ_s at a pressure head of ψ_{ae}, the effective water entry value, and f_{dF} is an as yet undetermined function of R_F. The dimensionless flux-conductivity ratio, R_F, is given by

$$R_F = q_F/K_s \tag{2}$$

where q_F is the flux through the finger defined by the flow rate through the finger, Q_F, divided by the cross-sectional area of the finger, A_F. Finger propagation velocity, v, is also a function of R_F given as

$$v = \frac{K_s}{(\theta_s - \theta_i)} f_{vF}(R_F) \tag{3}$$

where the function f_{vF} is again as yet undetermined.

The same analysis was applied to the larger chamber scale of a two-layer system by replacing the average flux through a finger, q_F, by the average flux through the entire system, q_S, defined by the flow rate through the system, Q_S, divided by the cross-sectional area of the system A_s. Instead of R_F at the chamber scale the dimensionless group R_S is defined

$$R_S = q_s/K_s \tag{4}$$

resulting in

$$\bar{d} = \frac{S^2}{(\theta_s - \theta_i)K_s} f_{dS}(R_S) \tag{5}$$

$$\bar{v} = \frac{K_s}{(\theta_s - \theta_i)} f_{vS}(R_S) \tag{6}$$

where $\bar{d}$ and $\bar{v}$ denote chamber scale averages and f_{dS} and f_{vS} are as yet undetermined. Note that R_S and R_F can be related by

$$\overline{R_F} = \beta R_S \tag{7}$$

where $\overline{R_F}$ is defined using the average flux through the fingers that form in the chamber, $\overline{q_F}$. Here β is defined as $A_S/n\overline{A_F}$ where n is the number of fingers, $\overline{A_F}$ is the average cross-sectional area of the fingers (or width in two dimensions), and A_S is the cross-sectional area of the system (or width in two-dimensional flow). As shown later, β is a function of $\overline{R_F}$.

The functional relationships given in (1), (3), (5), and (6) may be fitted to experimental data to determine the unknown functions and verify the $S^2/[(\theta_s - \theta_i)K_s]$ scaling of finger width and the $K_s/(\theta_s - \theta_i)$ scaling of finger velocity. As emphasized in P1, experiments must be designed and executed carefully with special emphasis on achieving porous medium isotropy and homogeneity. This paper presents the results of experiments that determine $f_{dF}(R_F)$, $f_{vF}(R_F)$, $f_{dS}(R_S)$, and $f_{vS}(R_S)$ for two-dimensional, unstable flow fields that develop in initially dry, fine-over-coarse layered-sand

[1]Now at Geoscience Analysis Division, Sandia National Laboratories, Albuquerque, New Mexico.

Paper number 89WR00270.
0043-1397/89/89WR-00270$05.00

systems, R_S, and thus R_F, is systematically varied through the texture of the top layer while the texture of the bottom layer, where instability occurs, is held constant. The results are compared with those obtained for a less homogeneous porous medium by *Hill and Parlange* [1972] and the theoretical results of *White et al.* [1976] and *Parlange and Hill* [1976].

EXPERIMENTAL METHOD

In the present study, methodology is extremely important because unstable phenomena are very sensitive to initial and boundary conditions. Since ambiguity resulting from different methodologies may yield misleading interpretations, a description of experimental procedures that addresses system sensitivity is warranted. Additional description can be found in the work by *Glass* [1985]. In general, requirements of the packed sand constituting the experimental porous media are (1) homogeneity and isotropy in pore structure (i.e., grain size distribution and bulk density) and uniform contact angle yielding homogeneous, isotropic macroscopic properties of conductivity and moisture characteristic relations, and (2) reproducibility.

Sand Preparation Procedure

White silica sand used commercially for sand blasting was dry seived through a nesting sequence of 8-inch wire mesh sieves (US sieve series numbers 14, 20, 30, 40, 50, 60, 80, 100, 140, 200) by a mechanical shaker yielding 10 sands of differing mean grain size and narrow distribution. These 10 sands allowed systematic variation in the macroscopic composite properties of the porous medium. The sand fractions in this paper are indicated by the sieves which bracket them.

In preliminary experiments it was discovered that the "dirtiness" of the sand, due to dust or clay that may be rinsed off and due to substances (such as oil or surfactant) on the sand surfaces themselves, greatly influenced the capillary properties of the "pack." To assure uniform contact angle across all the sands, each sand was boiled in a 0.5% solution of laboratory glass cleanser for 0.5 to 0.75 hours. The sand was then rinsed with warm tap water 15 times, boiled in tap water for an additional 15 min, and then wet sieved for 1 min with tap water. After five additional rinses with distilled water, the sand was dried at 60°C. The dry, clean sand was protected from contamination from air born particles until use; however, no effort was made to keep its moisture content from equilibrating with ambient humidity.

Two-Dimensional Slab Infiltration Chamber

A two-dimensional infiltration chamber was constructed out of clear plexiglas in "slab" sections 10 cm high with internal width 30 cm (side to side) and depth 1 cm (front to back). The slab sections were assembled in a frame with spacers between them to form small gaps that enable air to escape freely (small enough that the coarse sand can not escape and large enough that water does not enter them during an experiment). The sections also allowed sampling of bulk density with depth. A bottom "drip section" was constructed so that the flow through individual fingers could be monitored. The bottom drip section was divided into 10 compartments 3 cm wide across its entire 30 cm width by thin metal barriers higher than the capillary rise of the bottom layer sand. A hole in the bottom of each compartment was connected to a tube to monitor the distribution of flow out the bottom of the chamber.

TABLE 1. Two-Dimensional Experiments

Run No.	Size Fraction of Top Layer*	R_s	No. of Fingers	% Chamber in Fingers	Q_F Average, cm²/min
1	<200	0.007	4	21	1.9
2	<200	0.009	4	19	2.5
3	<200	0.012	4	19	3.3
4	100–140	0.038	4	24	10.9
5	100–140	0.041	5	20	9.3
6†	100–140	0.052	5	25	11.7
7	60–80	0.088	5	37	19.9
8†	60–80	0.11	6	33	20.8
9	50–60	0.14	4	37	40.8
10	40–50	0.28	6	65	53.8
11†	40–50	0.32	5	55	71.8
12	20–30	0.82	2	90	466

*Numbers refer to U.S. sieve series that bracket the fraction.
†Experiments part of set reported in the work by *Glass et al.* [1987].

Filling and Packing Apparatus

Preliminary experimental runs [*Glass et al.*, 1988] showed heterogeneities due to the segregation of the sand by size as the experimental chamber was filled and packed. Such heterogeneities were also noted in the studies of *Hill and Parlange* [1972] and *White et al.* [1976]. In addition to a homogeneous medium, a sufficiently dense medium is also necessary so that grains cannot move during the course of an experiment. If the sand is not tight, water running through fingers pulls the sand at their edges apart from the rest of the sand mass creating a small crack that prevents subsequent lateral movement of water from the fingers. To achieve the homogeneous, tight sand layer required, fully mixed sand was poured evenly across the top of a 68-cm-high chamber extension that fits above the slab chamber. The extension contains two coarse wire mesh grates, one at the bottom (between it and the top of the chamber) and one 10 cm from the bottom, that act as falling sand "randomizers." The sand rises evenly within the chamber and avoids the micro layering due to particle size segregation which occurs using most filling techniques in slab chambers. In addition to creating a homogeneous layer, the "peppering" action of the falling grains on the rising sand surface within the chamber provides a very tight pack as well. A dense pack was assured by lifting the filled chamber 1.5 cm and dropping it 200 times. Using this procedure an average porosity of 42% was found for the bottom 14–20 sand fraction layer. The top 10 cm or more of sand was removed until the bottom layer was 81 cm high with its top as flat as possible. A thin piece of cotton cloth was then placed on top of the bottom layer to keep fine particles from filtering down into the bottom layer and standardize the pore geometry of the textural interface. The top layer was then added and packed, and the top 10 cm or more was removed until it was 8 cm high.

Flux-Conductivity Ratio Experiments

We explored the effect of the flux-conductivity ratio for the finger, R_F, and the system flux-conductivity ratio, R_S, on

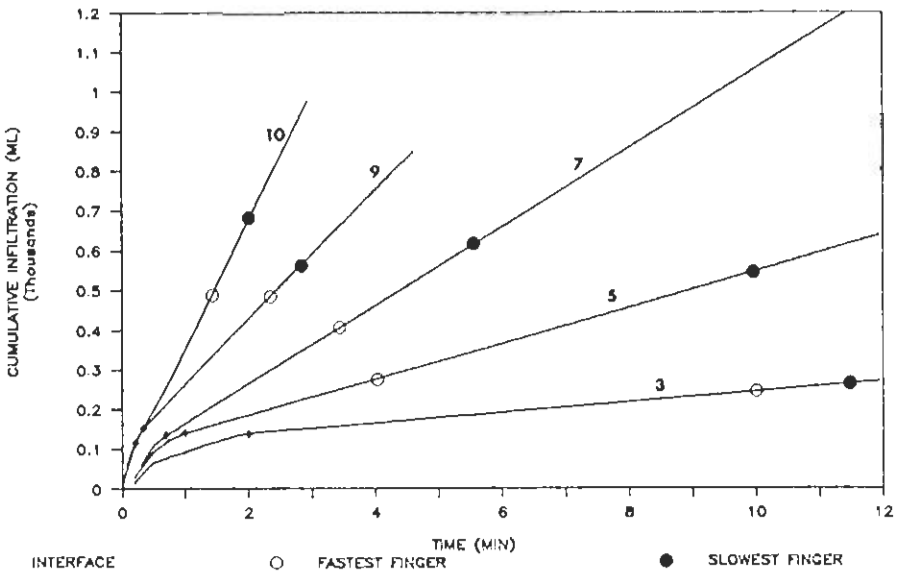

Fig. 1. Cumulative infiltration as a function of time for experiments 3, 5, 7, 9, and 10. Three times along each line are noted: when the wetting front crossed the textural interface and when the fastest and slowest moving fingers reached the bottom of the chamber.

the flow field in a bottom layer composed of the 14–20 sand fraction. Twelve experiments were conducted using six different finer textured top layers (see Table 1) thus varying R_S from 0.007 to 0.82. By measuring the width and flow rate through individual fingers, R_F spanned from 0.1 to 0.9. Since the widths of all fingers in the preliminary experiments conducted with the 14–20 bottom layer were greater than 1 cm, the 1-cm space between the walls of the slab infiltration chamber forced a two-dimensional flow field.

Distilled water with a low concentration of nonadsorbing dye (0.025% solution of USDA Red no. 3) was used in all experiments. The experiments were started by ponding the fluid to 1.5 cm quickly and evenly across the top of the fine textured layer through a plastic pipe containing many small holes. A pump supplied fluid to the plastic pipe and the depth of ponding was maintained constant throughout the duration of each experiment by a take-off tube that was connected back to the pump.

Flow field data were recorded with time lapse photography on movie film. Data were taken from the film by projecting it onto a screen and then tracing the wetting front position with time on acetate sheets. The newly wetted area and vertical length of each finger were measured from the film at minute or half minute intervals once fingers had moved into the bottom layer 3–10 cm. Finger widths for each time interval were calculated by dividing the wetted area by the finger length. The flow out the bottom of the chamber was measured through the 10 ports of the drip section. In experiments 3, 4, 5, 7, 9, 10, and 12 the flow into the chamber was also monitored in time.

RESULTS

The total flux through the two layer system with a coarse bottom layer is controlled principally by the conductivity of the more restrictive top layer, its vertical thickness and the ponding level [*Hill and Parlange*, 1972]. The cumulative inflow volume of water for experiments 3, 5, 7, 9, and 10 is plotted in Figure 1. The three points on each curve correspond to the wetting front crossing the textural interface and the arrival times of the fastest and the slowest fingers at the bottom of the chamber. From Figure 1 it is clear that the infiltration process at the surface is essentially controlled by the more restrictive top layer. Once the wetting front crosses the interface the infiltration rate becomes constant, indicating that the pressure gradient across the fine layer is constant in time. The bottom boundary condition which simulates a constant level water table also has no effect on cumulative infiltration at the soil surface when, as in our experiments, air can escape freely.

Drawings of the wetting front position in time for five experiments that span the range of R_S are shown in Figures 2*a* through 2*e* in order of increasing R_S. Several effects of R_S may be seen directly in these drawings. From a qualitative point of view, fingers meander in the horizontal more as R_S decreases. Quantitatively, R_S influences the velocity of fingers, their width, and the flow rate through fingers and thus R_F.

The widths and velocities obtained from each time interval measurement are plotted against each other in Figure 3. The pluses represent fingers which ran down in contact with the extreme left or right edge of the chamber (e.g., see Figure 2). These "side" fingers tend to be slightly narrower and faster moving than those that traverse the main body of the chamber and so are not considered in the following discussion. The remaining 100 points show a narrow band about a line whose slope is gradually decreasing as the finger width increases. The measurements on each finger are averaged to obtain a single width and velocity for each finger to be used in the evaluation of the relationships presented in the introduction.

Along the lines of the dimensional analysis presented in P1, the results of the experiments are analyzed on two scales: the finger scale and the two-layer system or chamber scale.

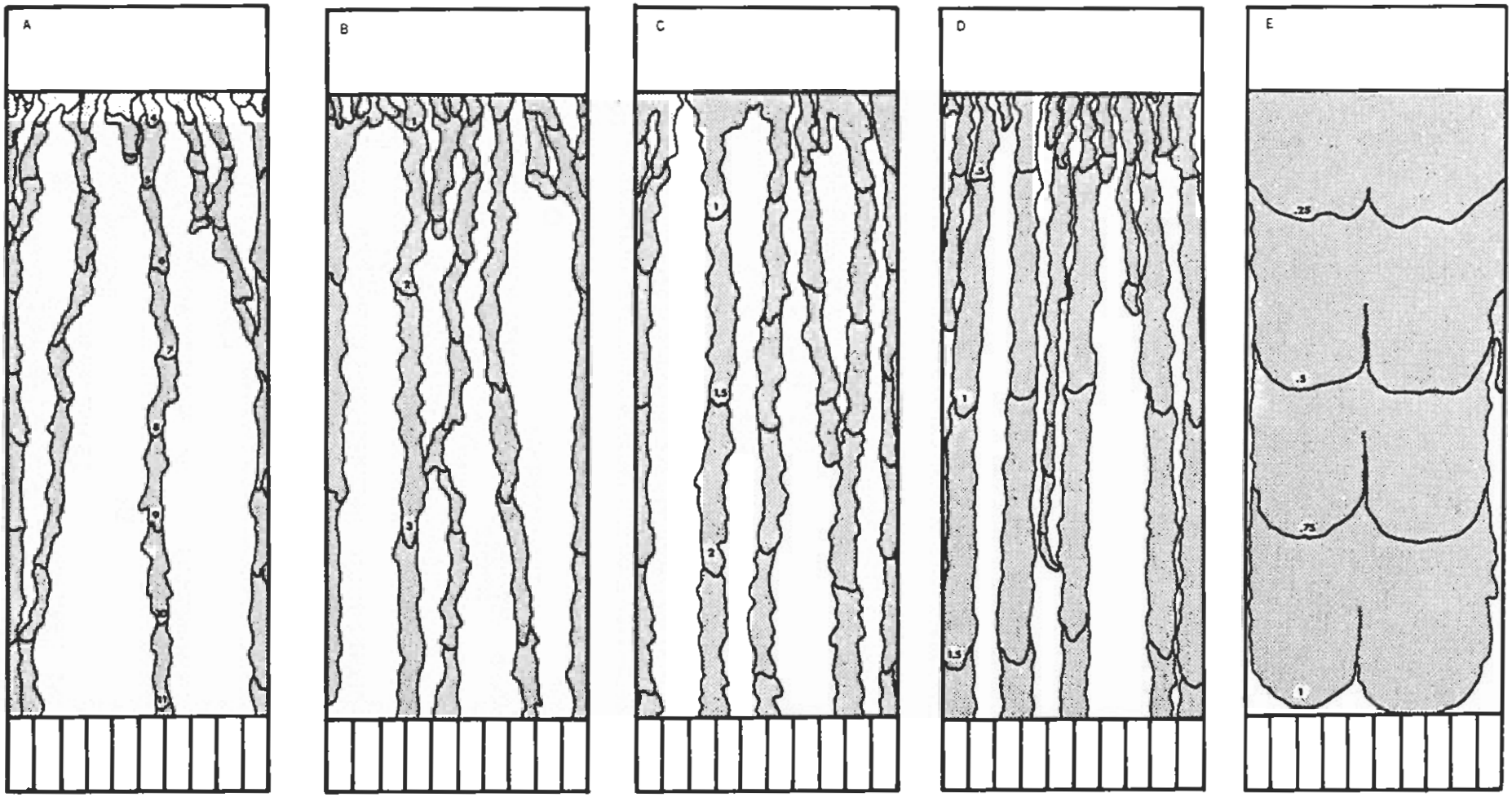

Fig. 2. Drawings of wetting front position in time after the start of infiltration for (a) experiment 3 (R_s = 0.012), (*b*) experiment 5 (R_s = 0.041), (*c*) experiment 7 (R_s = 0.088), (*d*) experiment 11 (R_s = 0.32), and (*e*) experiment 12 (R_s = 0.82). Numbers next to a wetting front position along a finger are in minutes. The small top rectangle is the fine top layer where the wetting front was stable.

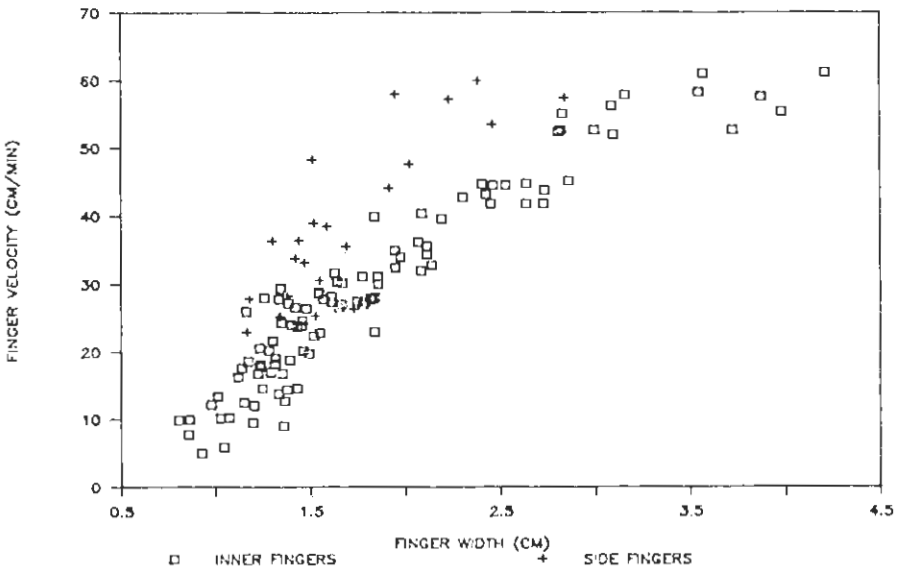

Fig. 3. Finger velocity, v, as a function of finger width, d, for all measurements. Pluses are measurements on fingers that ran along one of the sides of the chamber.

Finger Scale

On the finger scale we look for relationships between finger width, velocity, average moisture content, the flow rate through the finger and R_F. Since our experimental system is two dimensional, flow rates are given per unit depth (front to back) of the chamber and so have dimensions of square centimeters per minute. Figures 4, 5, and 6 show the effect of the flow through the finger, Q_F, on the finger propagation velocity, average moisture content, and width, respectively. The average moisture content for a finger is calculated by dividing the flow rate through the finger by the volume wetted per unit time. Often, more than one finger contributed to a drip section. Only fingers whose flow could be measured unambiguously are included in the plot. In addition, side fingers and fingers that merged near the bottom were discarded. As a result, only 16 of the 54 fingers that formed in the 12 experiments could be included. The plots show that finger velocity, average moisture content, and width all are higher when Q_F is higher.

The slope of finger velocity versus Q_F steadily decreases and the velocity asymptotically approaches the saturated pore velocity given by $K_s/(\theta_s - \theta_i)$ (Figure 4). The relationship between finger velocity and R_F is found to be a straight line throughout the full range of R_F between 0.1 and 0.9 covered in the experiments with the least squares best fit line given by $v = 79.2R_f + 7.82$ and an r^2 coefficient of 0.99. The velocity evaluated at $R_F = 1$ (87 cm/min) gives the value v should approach asymptotically. This value compares closely to the measured saturated pore velocity of 88 cm/min.

The average moisture content increases rapidly at low Q_F, then levels off and approaches the saturated value, θ_s, at high Q_F (Figure 5). The porosity, calculated to be 0.42 from bulk density measurements, also compares closely to the level attained above a Q_F value of about 100 cm^2/min.

Finger width also increases linearly with Q_F. This relation given by

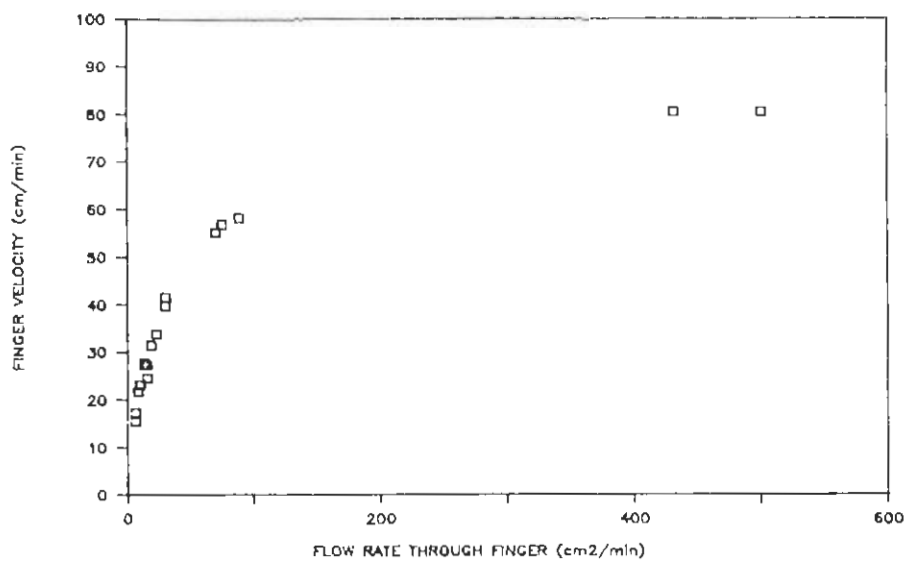

Fig. 4. Finger velocity, v, as a function of the flow rate through the finger, Q_F.

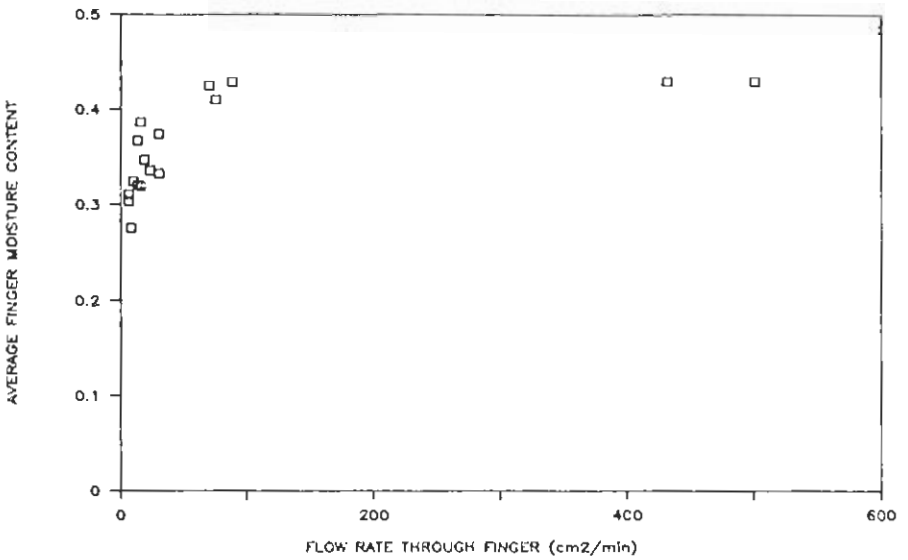

Fig. 5. Finger moisture content, θ_f, as a function of the flow rate through the finger, Q_f.

$$d = m_1 Q_F + b_1 \tag{8}$$

may be interpreted as follows. In the limit of Q_F large, b_1 may be neglected and we find $1/m_1 = Q_F/d$. Since θ approaches θ_s and v approaches K_s/θ_s for Q_F large then, Q_F/d must approach K_s. Thus $m_1 = 1/K_s$ and substitution into (8) yields

$$d = Q_F/K_s + b_1 \tag{9}$$

To write (9) in terms of the nondimensional finger flux-conductivity ratio R_F, we divide by d, recognize Q_F/dK_s as R_F and solve for d yielding

$$d = b_1/(1 - R_F) \tag{10}$$

Comparison of (10) and (1) both evaluated at $R_F = 0$ shows that b_1 should be given by

$$b_1 = S^2/[(\theta_s - \theta_i)K_s]f_{dF}(0) \tag{11}$$

where $f_{dF}(0)$ means the limit of f_{dF} for $R_F > 0$ but very small. For the 14–20 sand, K_s was measured to be 37.8 cm/min using a constant head permeameter. Since S^2 is very difficult to measure directly for coarse sands, the scaling theory of *Miller and Miller* [1956] is used to first obtain S_0^2 (the value of the sorptivity for a supply potential of zero) from measurements in finer (but similar) sand. S_0^2 is thus estimated from the 40-50 sand to be 80 cm^2/min (keeping only one significant figure in this estimation). In order to find the value of S^2 for a supply potential of $\psi_{w.c}$, we use the approximate formula for S_0^2 of *Parlange* [1975]

$$S_0^2 = \int_{\psi_c}^{0} (\theta + \theta_s - 2\theta_i)\, K\, d\psi \tag{12}$$

where θ_s is at a pressure of zero. This integral may be conveniently divided into two parts since K is constant for

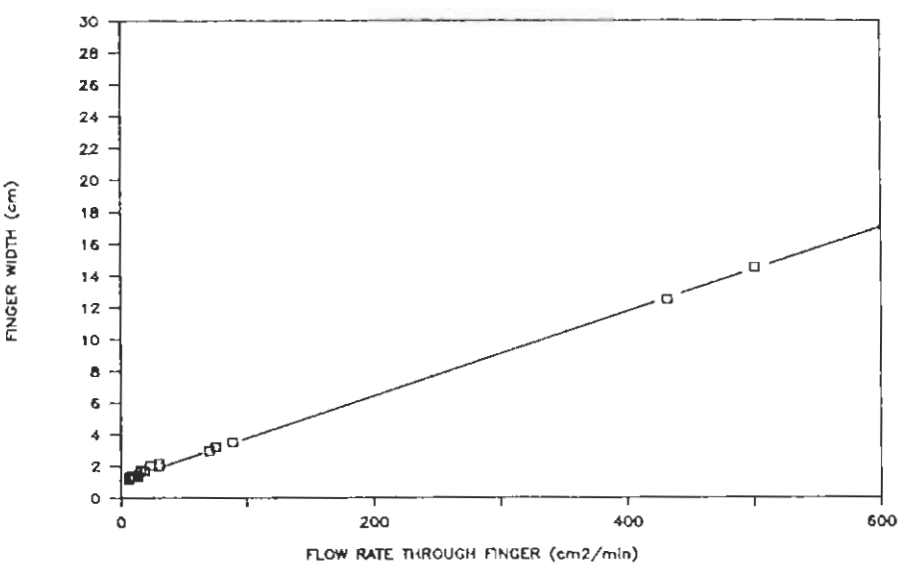

Fig. 6. Finger width, d, as a function of the flow rate through the finger, Q_f. The solid line is the least squares best fit line to the data.

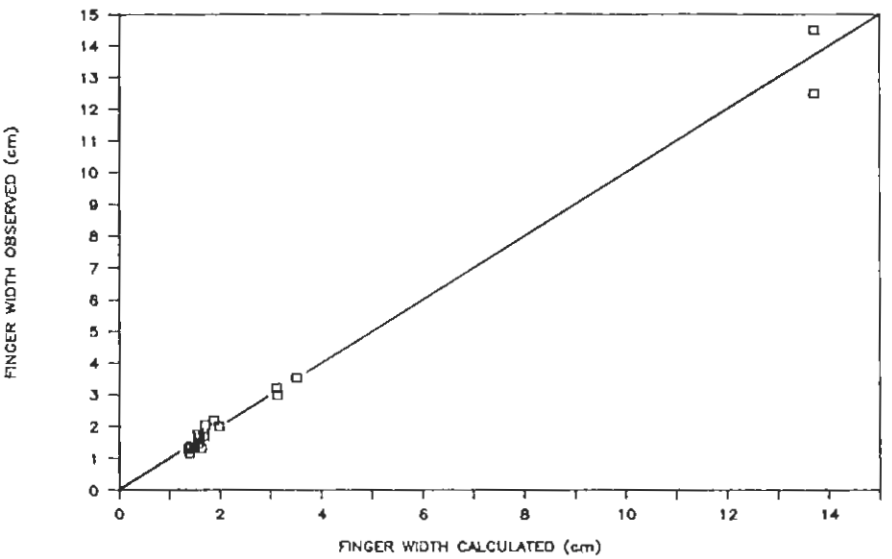

Fig. 7. Observed finger width, d, versus (15). Line drawn shows 1:1 correspondence.

$\psi > \psi_{we}$. Since $D\,d\theta = K\,d\psi$ and the value of ψ at θ_s is ψ_{we} we have

$$S_0^2 = \int_{\theta_i}^{\theta_s} (\theta + \theta_s - 2\theta_i)\, D\, d\theta - 2K_s\psi_{we}(\theta_s - \theta_i) \quad (13)$$

or

$$S_0^2 = S^2 - 2K_s\psi_{we}(\theta_s - \theta_i) \quad (14)$$

ψ_{we} was both measured and predicted by the method of *Haverkamp and Parlange* [1986] to be about −2.3 cm for the 14-20 sand. Taking θ_i as zero (air dry sand) and θ_s as the measured value of 0.42, S^2 is calculated to be 7 cm^2/min. A least squares best fit line to the data in Figure 6 gives m_1 as 0.0265 and b_1 as 1.19 with an r^2 of 0.999. The value for K_s obtained from m_1 is 37.78 cm/min, which is the same as that measured directly (37.8 cm/min). Using (11), $f_{dF}(0)$ is calculated to one significant figure as 3. Thus in the form of (1) we have

$$d = 3S^2/[(K_s(\theta_s - \theta_i)(1 - R_F)] \quad (15)$$

A plot of observed d versus the right-hand side of (15) is shown in Figure 7. As expected, given Figure 6 and (8), (15) is a good predictor of d.

The product of finger width and velocity plotted versus the flow through a finger is also a straight line (Figure 8). This relation given by

$$dv = m_2Q_F + b_2 \quad (16)$$

may be used to obtain v in the form of (3). Again as Q_F becomes large and b_2 may be neglected then $Q_F = dv/m_2$. For large Q_F the finger should be saturated so that $Q_F = dv(\theta_s - \theta_i)$ and thus $m_2 = 1/(\theta_s - \theta_i)$. Substituting for m_2 and rearranging gives

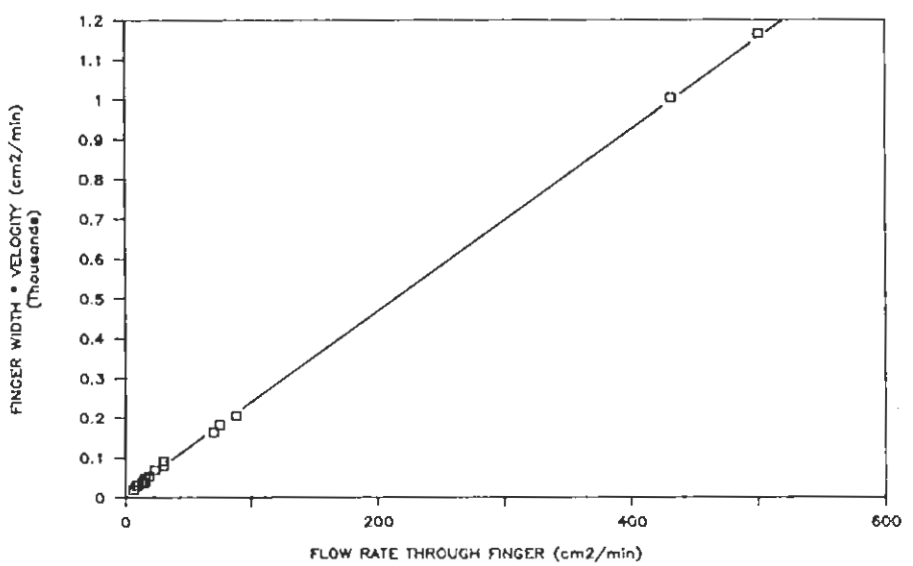

Fig. 8. Finger width times velocity, dv, as a function of flow rate through the finger, Q_F. The solid line is the least squares best fit line to the data.

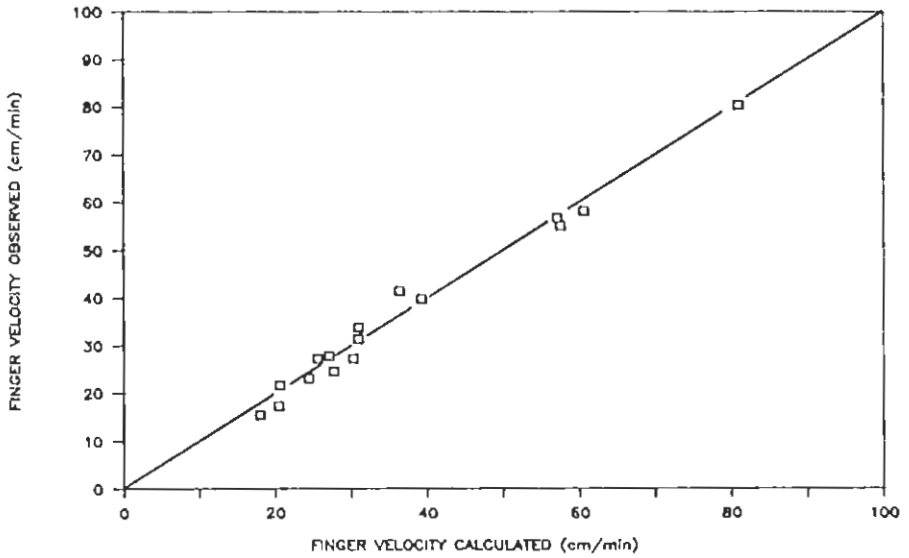

Fig. 9. Observed finger velocity, v, versus (22). Line drawn shows 1:1 correspondence.

$$v = \frac{q_F}{(\theta_s - \theta_i)} + b_2/d \tag{17}$$

Substitution of (10) for d yields

$$v = \frac{q_F}{(\theta_s - \theta_i)} + \frac{b_2}{b_1}(1 - R_F) \tag{18}$$

and writing in the form of (3) we have

$$v = \frac{K_s}{(\theta_s - \theta_i)}\left[\frac{b_2(\theta_s - \theta_i)}{b_1 K_s} + R_F\left(1 - \frac{b_2(\theta_s - \theta_i)}{b_1 K_s}\right)\right] \tag{19}$$

While it is clear that finger velocity will be zero when $R_F = 0$, our data suggest that for R_F small but positive, v approaches a limit v_{min} which is nonzero. The constant b_2 should be a product of the minimum finger area given by b_1 and v_{min} given by

$$v_{min} = C_2 K_s/(\theta_s - \theta_i) \tag{20}$$

where C_2 is simply the fraction of the maximum velocity that constitutes v_{min}. Thus

$$b_2 = b_1 C_2 K_s/(\theta_s - \theta_i) \tag{21}$$

and substitution into (19) yields

$$v = \frac{K_s}{(\theta_s - \theta_i)}[C_2 + R_F(1 - C_2)] \tag{22}$$

A least squares best fit line to the data in Figure 9 gives m_2 as 2.3 and b_2 as 9.2 with an r^2 of 0.999. Using the values of K_s and $(\theta_s - \theta_i)$ given above, C_2 is calculated to be 0.1. A plot of observed v versus the right-hand side of (22) is shown in Figure 9 and indicates (22) to be remarkably good. Again, this is expected, since the data presented in Figure 8 is well described by (16). Note that in the current formulation the finger velocity corresponds to $K(\theta_F)/\theta_F$, thus the conductivity function can be obtained by measurement of θ_F and v.

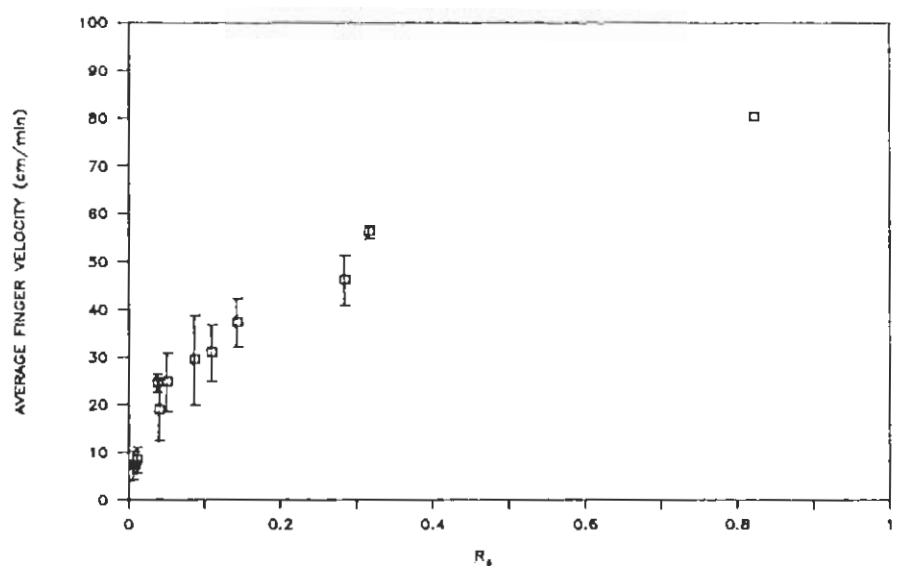

Fig. 10. Average finger velocity for an experiment, $\bar{v}$, as a function of the system flux-conductivity ratio, R_S. Bars denote plus or minus standard deviation.

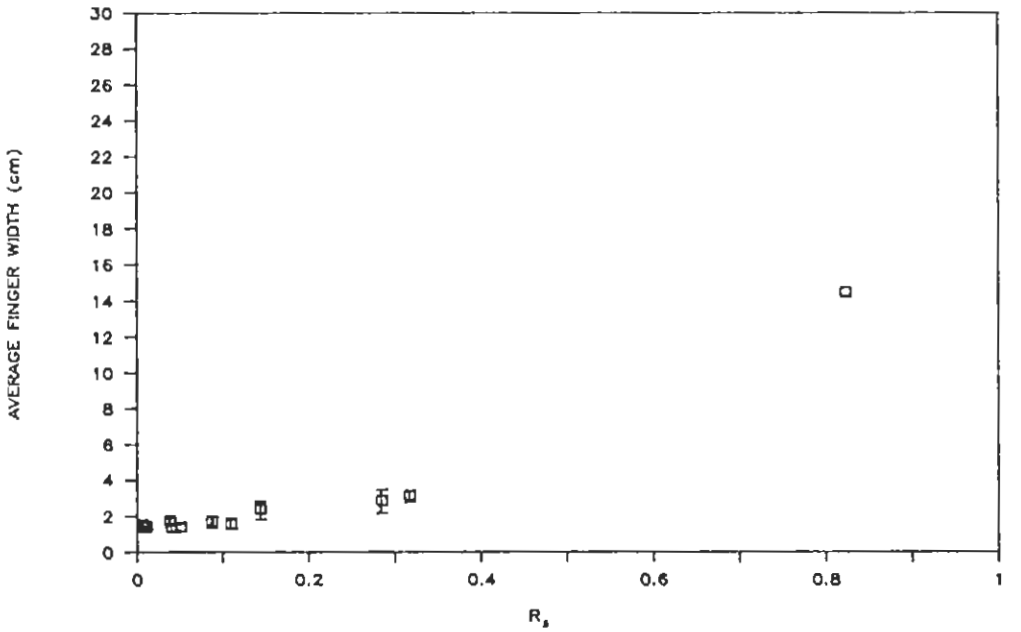

Fig. 11. Average finger width for an experiment, $\bar{d}$, as a function of the system flux-conductivity ratio, R_S. Bars denote plus or minus standard deviation.

Chamber Scale

On the chamber scale we look at the number of fingers and the average flow rate through fingers, the average finger width, and the average finger velocity all as functions of R_S. Average in the sense of the chamber scale will mean average for a particular experiment. As can be seen from Table 1, the number of fingers remains essentially constant as R_S is increased through moderate values. At high R_S the number of fingers should decrease eventually to one large finger occupying the entire chamber with the approach of one dimensional flow. This behavior is illustrated for an R_S of 0.8 in experiment 12 (Figure 2*e*) where two fingers formed and occupied 90% of the chamber width. The current experiments show that the width of fingers and the flow per finger increases with R_S. Table 1 shows this increase in terms of the percent of chamber width containing fingers and average flow per finger.

The average width and average velocity of fingers that formed in each experiment are plotted versus R_S in Figures 10 and 11. Only fingers which crossed into the bottom drip section and did not interact with the sides of the chamber were used to determine the average and standard deviation of the plots. For experiment 12 only two wide fingers formed and so a standard deviation was not calculated. Both figures show the same behavior as was seen at the finger scale: average width has a steadily increasing slope and average velocity has a steadily decreasing slope with R_S.

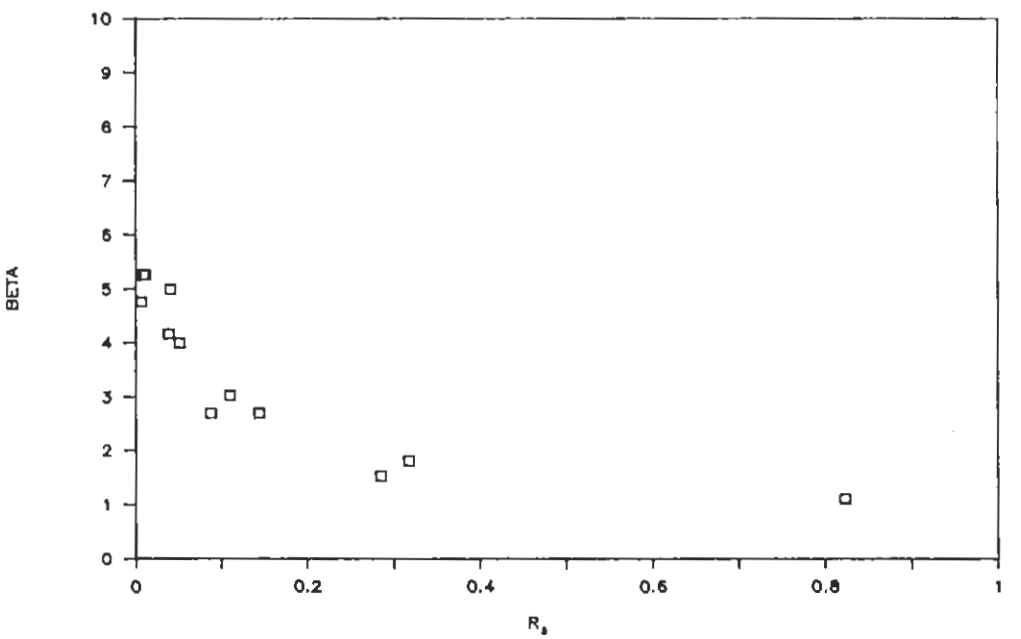

Fig. 12. β as a function of the system flux-conductivity ratio, R_S.

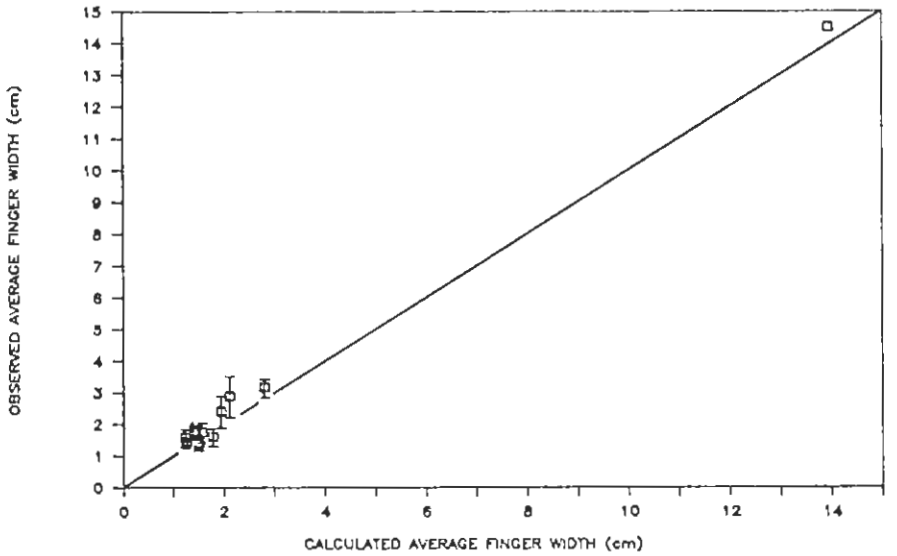

Fig. 13. Observed average finger width for an experiment, $\bar{d}$, versus (23). Line drawn shows 1:1 correspondence.

The same straight line relationships shown in Figures 6 and 9 may also be formed using average width, velocity, and flow rate through fingers for each experiment. The relations for finger width and velocity are most easily formed in terms of the average $\overline{R_F}$ for an experiment and then converted to R_S using (7). Thus we have (see equations (15) and (22))

$$\bar{d} = 3S^2/[K_s(\theta_s - \theta_i)(1 - \beta R_S)] \tag{23}$$

$$\bar{v} = \frac{K_s}{(\theta_s - \theta_i)}[C_2 + \beta R_S(1 - C_2)] \tag{24}$$

β, the conversion factor between $\overline{R_F}$ and R_S defined in (7), is itself a function of R_S as is shown in Figure 12. Observed $\bar{d}$ and $\bar{v}$ versus the right-hand sides of (23) and (24) are shown in Figures 13 and 14, respectively. Again, the predictive capability of (23) and (24) is quite good.

DISCUSSION

The effect of the flux-conductivity ratio on the behavior of the unstable wetting front may be summarized as follows. At the chamber scale, as R_S increases, the number of fingers per width of chamber is not greatly affected. However, the average flow through the finger, finger width, and finger velocity all increase and the percent of the chamber containing fingers increases. At the finger scale, with the increase in flow through a finger, finger width, velocity, and moisture content all increase.

These results are different from those found experimentally by *Hill and Parlange* [1972]. In five experiments where R_S was changed between two levels, 0.07–0.08 and 0.10–0.11, they found that increasing R_S increased the number of fingers that formed but did not effect their velocity or cross-sectional area. In addition, the velocities of all the fingers were close to the saturated pore velocity. The difference between our and Hill and Parlange's results are most likely due to differences in heterogeneity structure within the bottom layer.

Heterogeneities in porous media properties on the macroscale which modulate the average pore size in space are

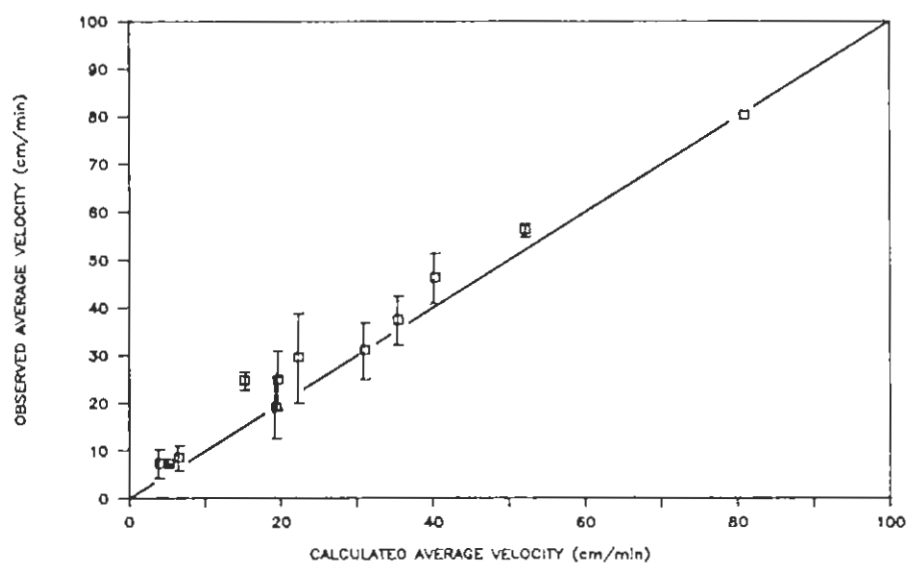

Fig. 14. Observed average finger velocity for an experiment, $\bar{v}$, versus (24). Line drawn shows 1:1 correspondence.

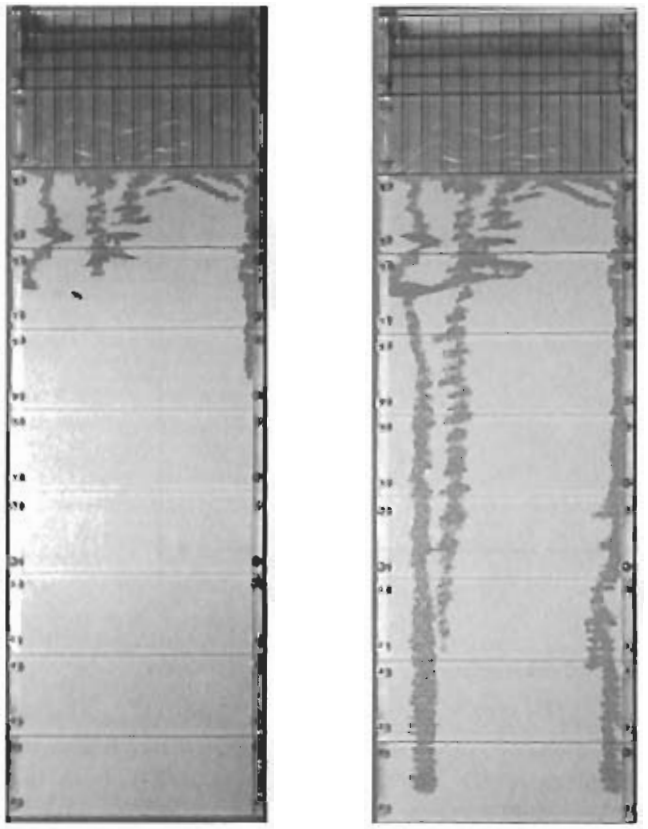

Fig. 15. Preliminary fine-over-coarse layer experiment demonstrating the importance of slight heterogeneities in finger meandering and merger.

important in determining the direction taken by fingers and their meandering which enhances merger. These effects are demonstrated clearly in the sequence of two photographs shown in Figure 15 taken of a preliminary experiment before the development of the filling and packing techniques. The heterogeneities responsible for the complicated pattern within the top of the bottom layer could barely be detected by eye. The intention in the present laboratory experiments was to remove as many of the heterogeneities as possible so the fingering phenomenon could be studied in the absence of their complications. Heterogeneities were, however, still present and responsible for the side to side meandering of fingers as can be seen in Figure 2.

From our results, meandering of the fingers appears qualitatively to be a function of the flow rate through the finger. Meandering decreases as the flow rate through the finger increases. The more a finger meanders, the more likely it will hit another finger and merge to create a wider faster moving finger. Since we have found that a lower system flow rate yields a lower individual finger flow rate, merger, and flow rate through the system are related, no matter the heterogeneity "intensity." When applied to a finite length column, a relationship between R_S and the number of fingers that reach the bottom of the column emerges. Our results show a very slight increase in the number of fingers that form with R_S followed by a decrease as R_S approaches 1. Parlange and Hill's results may be due simply to an increase in the heterogeneity intensity such that the relationships between system flow rate and merger for their finite length column is more sensitive than in our case. In addition, since there is a ceiling on the possible finger velocity, merger will eventually produce fingers which all move at the same top speed as they found.

It is obvious that the effect of heterogeneity level must be explored systematically. We are currently using an adaption of *Hoa*'s [1981] technique to determine heterogeneity in our chamber under different filling and packing techniques. Our preliminary results support our contention that the filling and packing methods developed and used in this study create porous slabs that are free of layering heterogeneity while those of all other methods tried (vibrational packing, tamping, pouring from funnel with back and forth motion, etc.) are not.

Another point of departure from Hill and Parlange is the presence of an "induction" zone beneath the textural interface in their experiments while in our case we do not see such a zone. Instead we observe the interface between the two layers to allow water to pass into the bottom layer at many discrete very regularly spaced locations or "point sources." The induction zone of *Hill and Parlange* [1972] could be due to fines from the top layer which filtered down into the bottom layer during filling. In preliminary experiments before we put cloth at the interface, fines always filtered down into the bottom layer and an induction zone was always present. Since fingers either develop in an induction zone or directly at the textural interface, it is important for future studies to carefully study this region in an effort to further understand the basic mechanism of finger formation. Here, we were interested in fully formed fingers because they very rapidly dominate the flow field and have been found to persist from one infiltration cycle to the next. Thus we standardized the finger formation zone by separating the layers with a piece of cloth so that only the flow rate into the bottom layer varied and not the geometry of the pore transition.

The quantitative results presented in (23) for $\bar{d}$ as a function of R_S may be compared to those derived through linear stability analysis and presented by *White et al.* [1976], and *Parlange and Hill* [1976]. In P1, these analytically derived formulations were manipulated into the form of (5), yielding d_W and d_P respectively (see equations (34) and (36), P1):

$$d_W = \pi\left(\frac{3\sigma}{\rho g(\theta_s - \theta_i)(1 - R_S)}\right)^{1/2} \tag{25}$$

$$d_P = \frac{\pi S^2}{K_s(\theta_s - \theta_i)(1 - R_S)} \tag{26}$$

Equation (25) yields a $(1 - R_S)^{-1/2}$ behavior which is not observed for our experiments; d_P, however, is identical to our results (equation (23)) for $\pi \simeq 3$ except for the factor β missing in (26). Given this encouraging correspondence between our experiments and Parlange and Hill's results, we explore their analysis more closely.

In deriving (26), *Parlange and Hill* [1976] assumed that the fingers were saturated and so took $q_f = K_s$ instead of the conductivity at the moisture content of the finger, K_f. Their analysis may be repeated without this restriction, i.e., assuming that the average water content in the finger is only equal to θ_f rather than θ_s, to yield

$$d_P = \pi S_f^2/[(\theta_f - \theta_i)K_f(1 - q_S/q_f)] \tag{27}$$

where S_f is the sorptivity evaluated for the moisture content of the finger, θ_f. As previously stated (see equations (8) and (9)) in P1, the combination $S_f^2/[(\theta_f - \theta_i)K_f]$ is a weak

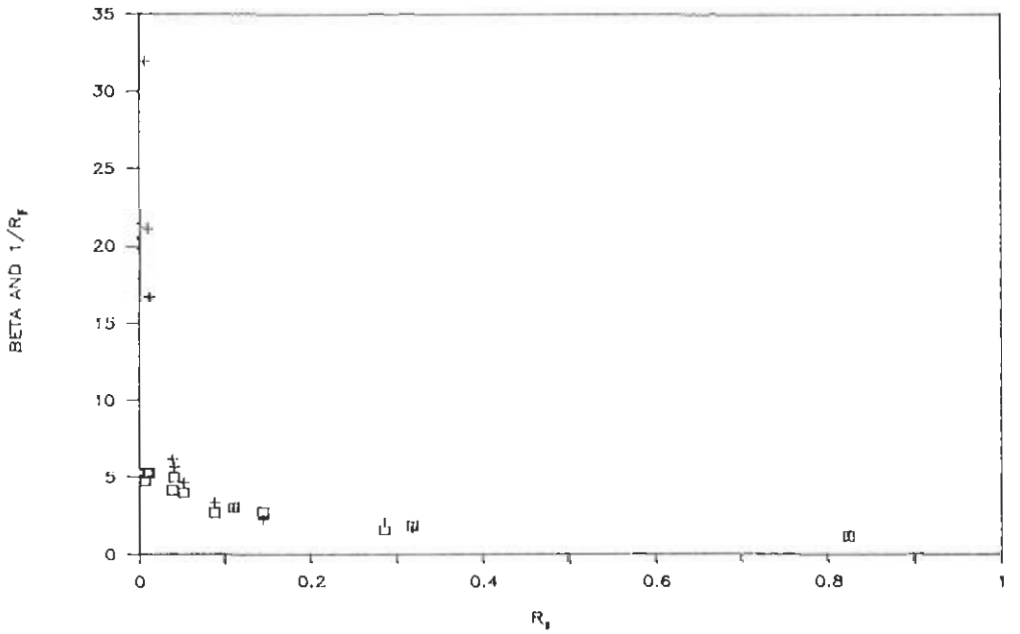

Fig. 16. The β (pluses) and $1/\overline{R_f}$ (boxes) versus R_s.

function of θ_f for θ_f near θ_s. Thus we can evaluate it assuming $\theta_f = \theta_s$ with only a small error.

Writing (27) in terms of $\overline{R_f}$ and R_s we have

$$d_p = \pi S^2 / [(\theta_s - \theta_i) K_s (1 - R_s / \overline{R_f})] \tag{28}$$

Equation (28) is consistent with (5), since R_s is a function of $\overline{R_f}$ given by (7). Comparison of (28) and (23) shows that linear theory predicts

$$\beta = 1/\overline{R_f} \tag{29}$$

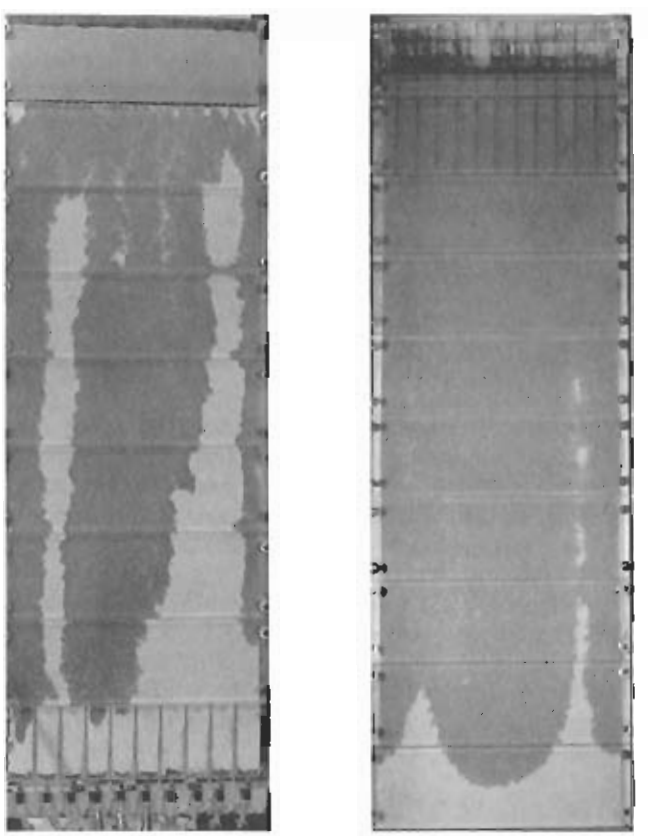

Fig. 17. Decreased mean grain size (40-50 sand) increases finger width as predicted by the scaling theory of *Miller and Miller* [1956]: (*a*) $R_s = 0.23$ and (*b*) $R_s = 0.6$.

Fig. 18. Precleaned, "dirty" 40-50 sand with the same R_s as in Figure 17 (right) shows the effect of decreased capillary forces to decrease finger width.

or that R_S and $\overline{R_F}$ are related as

$$R_S = \overline{R_F}^2 \tag{30}$$

Both β and $1/\overline{R_F}$ are plotted as functions of R_S in Figure 16. It is seen that (29) is approximately satisfied if R_S is not too small. As R_S approaches zero, however, β and $1/\overline{R_F}$ depart dramatically. This is not surprising, since the linear theory assumes wet fingers, whereas the fingers become dryer as R_S goes to zero. Even though β does not obey (29) as R_S approaches zero, (28) still predicts d accurately, since $R_S/\overline{R_F}$ becomes negligible in that limit anyway; i.e., the value of β is irrelevant for R_S small. On the other hand, as R_S goes to 1, (29) predicts β accurately; however, (28) becomes very sensitive to the exact value of $R_S/\overline{R_F}$ which also approaches 1. Apart from these extremes, (26) reduces to (15), and thus our results are entirely consistent with the theory of *Parlange and Hill* [1976] when their theory is properly interpreted in (28) and with the use of (30). The fact that agreement between the linear theory of Parlange and Hill and our experimental results is so close is likely due to the approximations used by Parlange and Hill in their linear stability analysis. While the analysis linearizes with respect to the perturbation so that only very small disturbances are treated, the fundamental nonlinearity in soil property is preserved.

To conclusively test the $S^2/[(\theta_s - \theta_i)K_s]$ scaling of finger diameter and the $K_s/(\theta_s - \theta_i)$ scaling of finger velocity, experiments must be conducted to vary the properties of the bottom layer systematically. We are in the process of conducting experiments where the mean grain size of the bottom layer is systematically varied while the log scale grain size distribution remains the same. Two of these experiments are shown in Figure 17 where R_S has been varied from 0.23 to 0.6, respectively, for a bottom layer composed of the 40-50 sand. As the theory predicts, finger widths are, indeed, larger than in the 14-20 sand reported in this paper (for the same R_S). These experiments will allow the testing of the Miller scaled forms of the equations for v and d proposed in P1. The scaling of finger diameter and velocity may also be tested within the same porous medium by influencing its capillary properties and thus its sorptivity. Figure 18 shows an identical experiment to that in Figure 17 (right) except that the 40-50 sand used in this experiment was precleaned, "dirty" sand which demonstrated a lower capillary rise than the cleaned 40-50 sand shown in Figure 17 (right). To address nonsimilar porous media we also are systematically varying the grain size distribution about one mean grain size. In addition, the effects of uniform initial moisture content on S^2, K_s, and θ_s and thus on finger width and velocity must be addressed in the laboratory. Finally, it is important to point out that while finger properties may most easily be observed in two-dimensional flow fields, the relationships found in this paper must be extended for the more applicable case of three dimensional unstable flow fields by appropriate experimentation.

CONCLUSION

Wetting front instability in initially dry, homogeneous porous media causes the formation of fingers that are unsaturated and have variable average moisture contents, velocities, widths, and flow rates. In this paper we present the results of experiments designed to determine the dependence of finger width and velocity on system parameters following the dimensional analysis of P1. We accomplish this for one particular near homogeneous porous medium and evaluate formulations for finger width and velocity as functions of R_F and R_S. Finger width is found to be closely approximated by linear stability analysis following *Parlange and Hill*'s [1976] work. The experimental observation that fingers are not saturated motivates a reinterpretation of Parlange and Hill's analysis that accounts for this fact and yields a relationship for the finger width that fits closely the behavior observed here. Thus we show that the correlation between linear stability theory and experiments in isotropic homogeneous porous medium where the theory should apply to be surprisingly good. The complications of heterogeneities can explain why the experiments of *Hill and Parlange* [1972] were not properly described by the theory. Heterogeneities cause the merger of fingers and the formation of faster, wider fingers, a process not accounted for directly in the linear theory. Because of the importance for field soils of heterogeneity in hydraulic properties, nonuniform initial moisture content and variable surface infiltration in both time and space, their effects on fingering must be addressed before results applicable to the field are obtained.

Acknowledgments. This research was supported in part by the Annual Allotment Program of the U.S. Department of Interior, EPA grant R81-2919-01-0, and the Department of Agricultural and Biological Engineering, Cornell University, Ithaca, New York. Special thanks is given to Pat Hasson, Stephen Cann, and Kathy Bliss for help conducting the experiments and processing data.

REFERENCES

Glass, R. J., A study of wetting front instability in layered porous media, M.S. thesis, Cornell Univ., Ithaca, N.Y., 1985.

Glass, R. J., J-Y. Parlange, and T. S. Steenhuis, Water infiltration in layered soils where a fine textured layer overlays a coarse sand, paper presented at Proceedings of the International Conference for Infiltration Development and Application, Jan. 5–9, Hawaii, 1987.

Glass, R. J., T. S. Steenhuis, and J-Y. Parlange, Wetting front instability as a rapid and far-reaching hydrologic process in the vadose zone, *J. Contam. Hydrol.*, *3*, 207–226, 1988.

Glass, R. J., J.-Y. Parlange, and T. S. Steenhuis, Wetting front instability, 1, Theoretical discussion and dimensional analysis, *Water Resour. Res.*, this issue.

Haverkamp, R., and J-Y. Parlange, Predicting the water-retention curve from particle-size distribution, 1, Sandy soils without organic matter, *Soil Sci.*, *142*, 325–329, 1986.

Hill, D. E., and J-Y. Parlange, Wetting front instability in layered soils, *Soil Sci. Soc. Am. Proc.*, *36*, 697–702, 1972.

Hoa, N. T., A new method allowing the measurement of rapid variations of the water content in sandy porous media, *Water Resour. Res.*, *17*(1), 41–48, 1981.

Miller, E. E., and R. D. Miller, Physical theory for capillary flow phenomena, *J. Appl. Phys.*, *27*, 324–332, 1956.

Parlange, J-Y., On solving the flow equation in unsaturated soils by optimization, Horizontal infiltration, *Soil Sci. Soc. Am. Proc.*, *39*, 415–418, 1975.

Parlange, J-Y., and D. E. Hill, Theoretical analysis of wetting front instability in soils, *Soil Sci.*, *122*, 236–239, 1976.

White, I., P. M. Colombera, and J. R. Philip, Experimental study of wetting front instability induced by sudden change of pressure gradient, *Soil Sci. Soc. Am. J.*, *40*, 824–829, 1976.

R. J. Glass, Geosciences Analysis Division 6315, Sandia National Laboratories, Albuquerque, NM 87185.

J-Y. Parlange and T. S. Steenhuis, Department of Agricultural and Biological Engineering, Cornell University, Ithaca, NY 14853.

(Received April 7, 1988;
revised January 17, 1989;
accepted February 1, 1989.)